ARTICLE

OPEN

Check for updates

Bio-inspired selective nodal decoupling for ultra-compliant interwoven lattices

Yash Mistry[1], Oliver Weeger[2], Swapnil Morankar [3], Mandar Shinde[1], Siying Liu[4], Nikhilesh Chawla[3], Xiangfan Chen [4], Clint A. Penick[5,6] & Dhruv Bhate [1✉]

Architected materials such as lattices are capable of demonstrating extraordinary mechanical performance. Lattices are often used for their stretch-dominated behavior, which gives them a high degree of stiffness at low-volume fractions. At the other end of the stiffness spectrum, bending-dominated lattices tend to be more compliant and are of interest for their energy absorption performance. Here, we report a class of ultra-compliant interwoven lattices that demonstrate up to an order of magnitude improvement in compliance over their traditional counterparts at similar volume fractions. This is achieved by selectively decoupling nodes and interweaving struts in bending-dominated lattices, inspired by observations of this structural principle in the lattice-like arrangement of the Venus flower basket sea sponge. By decoupling nodes in this manner, we demonstrate a simple and near-universal design strategy for modulating stiffness in lattice structures and achieve among the most compliant lattices reported in the literature.

[1] 3DX Research Group, Arizona State University, Mesa, AZ 85212, USA. [2] Technical University of Darmstadt, Darmstadt, Hesse, Germany. [3] School of Materials Engineering, Purdue University, West Lafayette, IN 47907, USA. [4] School of Manufacturing Systems and Networks, Arizona State University, Mesa, AZ 85212, USA. [5] Department of Evolution, Ecology & Organismal Biology, Kennesaw State University, Kennesaw, GA 30144, USA. [6] Present address: Department of Entomology and Plant Pathology, Auburn University, Auburn, Alabama 36849, USA. ✉email: dpbhate@asu.edu

Cellular materials such as honeycombs, foams, and lattices have expanded the range of high-performance materials available to engineers by their use of negative space and design to achieve properties that cannot be otherwise obtained[1,2]. The concurrent maturation of computational design tools and additive manufacturing processes has given rise to a new generation of architected cellular materials with extraordinary properties[3]. The design of architected cellular materials is often inspired by biological, crystallographic, or mathematically generated structures[4]. With regard to biologically derived, or bio-inspired cellular materials, the design principle that is typically abstracted from the natural structure is the topology of the unit cell itself[5]. However, closer examination of the features that constitute the unit cell often reveals finer details that are also worthy of abstraction. For example, a deeper study of the hexagonal cells of the honeybee's nest has revealed that secondary meso-structural features such as wall coping and corner radius have the functional benefits of increasing specific flexural rigidity and minimizing corner stress, respectively[6,7].

While a wide variety of cellular material topologies have been proposed and evaluated for several applications[8], there are many unresolved questions[9] with regard to the optimality of their design in real-world applications. Additionally, most of the functional interest for beam-based lattices, one of the most common forms of cellular materials, has been in regard to their ability to provide high stiffness-to-weight performance, where topology optimization approaches have been very successful[10]. A functional domain that has been less studied is compliance of lattice structures, which forms the focus of this work.

For this study, design inspiration was drawn from the Venus flower basket (*Euplectella aspergillum*), a deep-sea glass sponge from the class *Hexactinellida* that has received significant interest from the scientific and engineering communities over the past two decades[11]. Venus flower baskets are typically found in the Pacific and Indian oceans, and are covered in a mat of soft, filter-feeding tissue when alive. They usually grow at the depth of 100 to 1000 m where the temperature is between 2 and 11 °C and can survive for hundreds of years in these conditions. At these depths, the structure experiences lateral forces from water currents and is also under risk of predation by starfish and vertebrates, while having to manage the forces of swimming fish bumping into them. Given the inherently brittle nature of the silica-based material that the basket is mostly comprised of, it is remarkable that this structure has thrived in these conditions. It is hypothesized that this exceptional behavior is enabled by at least six hierarchical levels of design strategies at length scales ranging from nanometers to centimeters[12]. At the lower end of that length scale, the Venus flower basket is composed of needle-like structures called spicules, which in turn are made of concentric layers of silica laminates separated by organic interlayers that have been shown to arrest crack propagation[13]. These bundles of spicules are arranged to form a grid-like structure with a checkerboard pattern spanning the entire structure of the basket[14], as shown in Fig. 1a. This pattern is surrounded by helical ridges that have been shown to provide mechanical reinforcement and hydrodynamic benefits[15].

There are several design principles, such as the use of diagonal and helical reinforcements, that are embedded within the structure of the Venus flower basket[16–18], and have been proposed for bio-inspired design[13,14,19,20]. However, these reinforcements emerge at a later stage of maturity in the organism[12]. A closer inspection of the lattice structure of a not fully mature Venus flower basket (Fig. 1b, c), reveals that the struts comprising the lattice are not fully connected at each node (Fig. 1d), and are decoupled selectively. X-ray microscopy (Methods–X-ray Tomography) reveals that the Venus flower basket consists of
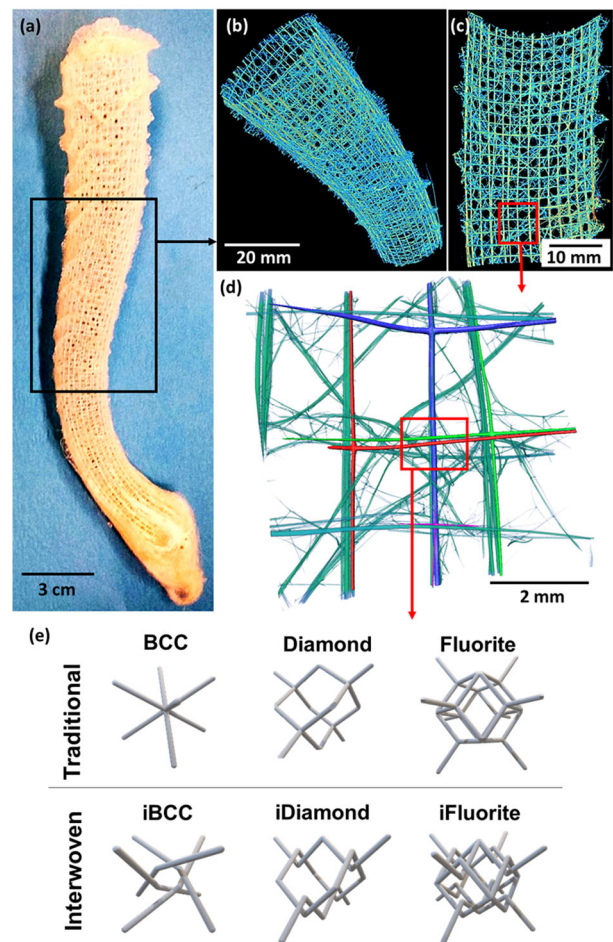

Fig. 1 Decoupled nodes in Venus Flower Basket as inspiration for designing interweaving lattices. The structure of the **a** Venus flower basket, while initially appearing like **b** a fully connected lattice, reveals on closer examination to have more of **c** a woven nature, with **d** struts making contact, but not fully connected to each other at every node, which inspired **e** the selective nodal decoupling concept and was applied to three different lattice shapes in this work.

independent lattice strut systems that are woven into each other, as shown with different color markers in Fig. 1d. None of the prior studies of the Venus flower basket's structure have adequately examined the benefits of this nodal decoupling.

This work abstracts[19] the underlying design principle of selective nodal decoupling to generate interwoven lattices from the structure of the Venus flower basket. The isolation of this design principle enables a more generalizable evaluation of its benefits on a range of existing lattice topologies such as Diamond, Fluorite and Body-Centered Cubic (BCC), as demonstrated in Fig. 1e. Compression tests demonstrate remarkable properties including an up to 20-fold increase in compliance when compared to fully connected (traditional) lattice structures.

Results
Three-dimensional (3D) woven materials have been studied previously for their use in composites[21], and textile-inspired approaches to 3D weaves are gaining increasing interest[22,23]. Woven structures have also been fabricated by three-dimensional weaving of wires, typically by brazing stacks of two-dimensional wire meshes[24,25]. In the context of additively manufactured architected cellular materials, interpenetrating lattices have been recently proposed, which demonstrate negative stiffness behavior,
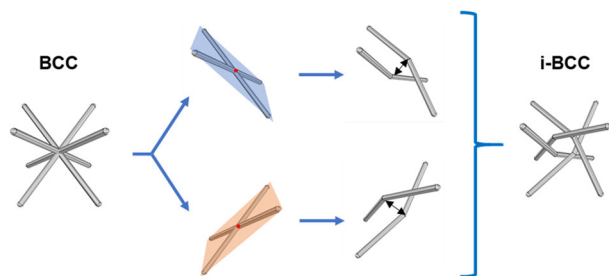
Fig. 2 Interwoven lattices designed by decoupling nodes in traditional lattices. BCC shown here, transforming it into an interwoven, or i-BCC lattice. The first step involves identifying the planes that contain struts intersecting at nodes. The struts at these nodes are separated perpendicular to the plane by a clearance distance, resulting in an interwoven lattice.

and the potential for electromechanical coupling[26]. Lattices with braided rope-like woven members have also been shown to have higher compliance than the ones with traditional beams, but these structures are challenging to manufacture at scale[27]. This work differs from these prior efforts in proposing a simple and generalizable approach to generating woven 3D structures by selectively decoupling nodes in traditional lattices, and in achieving unsurpassed compliance values for cellular materials.

To evaluate the interwoven lattice design principle, the BCC lattice was first selected as a baseline from which interwoven lattices were developed. The BCC lattice is a bending-dominated structure[28] (i.e. lattice deformation is primarily driven by beam bending as opposed to beam stretching) and is commonly used in studies of architected material behavior. To generate an interwoven structure, the BCC unit cell was split into two planes, each containing two pairs of struts that intersect at a node located at the centroid of the tessellated volume (Fig. 2, Supplementary Figure 1). The struts were then decoupled in opposite directions at the centroidal node, while keeping the newly created pair of nodes in the same plane. After this step, both pairs of struts were merged back to create an interwoven unit cell. The eight corner nodes were retained to ensure periodicity. Unit cells of the traditional BCC and its interwoven counterpart (i-BCC) were populated into 45 mm cubic specimens for compression testing (Methods—Design, Grasshopper design scripts available[29]).

Polyamide-12 (PA12) specimens were fabricated using a Selective Laser Sintering (SLS) additive manufacturing process[30] (Fig. 3a) with three different strut diameters: 1.2, 1.5, and 1.8 mm, and a unit cell size of 15 mm in X, Y, and Z-directions, sandwiched between 4 mm thick platens (Supplementary Figure 2, relative densities in Supplementary Table 1). Three replicates were fabricated at each of the three thicknesses (Methods—Manufacturing). These specimens were subjected to quasistatic compression (Supplementary Movie 1). The load-displacement curves for the BCC and i-BCC specimens are shown in Fig. 3b, c, respectively, with three curves for each design shown representing three replicates (Methods—Testing). The results show a significant, 21.5-fold reduction in the effective stiffness for i-BCC relative to traditional BCC lattices, even with similar relative densities (Supplementary Table 1). Additionally, the undulations in the plateau region of the BCC are significantly mitigated for the i-BCC.

To gain insight into the deformation mechanisms, the experiment was simulated using a numerical approach[31] that represents the struts as nonlinear, shear-deformable 3D beam elements (Methods—Simulation) and with an elasto-visco-plastic material model for PA12 (Supplementary Figure 3). The results are shown in Fig. 3d, e for the BCC and i-BCC specimens

respectively, showing good agreement, particularly given the existence of instabilities, contact, and inelastic material behavior. The internal force contours shown in Fig. 3d, e at an applied displacement of 13 mm (corresponding to 30% effective strain, which was estimated as the displacement applied to the top of the specimen divided by its initial height), reveal that the i-BCC has greater homogeneity in the distribution of forces through the lattice compared to the BCC (Supplementary Fig. 4). Additionally, the simulation results also agree with the experimental observation of greater localization of buckling in beams along failure bands for the BCC relative to the i-BCC. Localization of failure along these bands causes load drops and results in undulations in the stress plateau during compression. The absence of these bands for the i-BCC explains why it has a smoother plateau (Fig. 3c, Supplementary Fig. 5). Thus, the key benefits to the compression response from decoupling nodes in a BCC lattice are (i) a significant increase in its compliance, (ii) a reduction in the undulations present in the compression plateau, and (iii) a reduction in the internal forces generated within the lattice struts.

To examine the generality of selectively decoupling nodes to enhance compliance, three additional lattice structures, viz. diamond, flourite, and a hybrid lattice comprised of BCC and FCC (Face-Centered-Cubic) lattices were studied. These lattices had the same strut diameters as before (relative densities in Supplementary Table 1). In principle, any lattice structure with nodes in the interior of the tessellation volume can be converted into an interwoven lattice using the approach developed here. Nodes on the tessellation surface including the corners and edges, if decoupled, would violate boundary periodicity, an inherent requirement for a unit cell if it is to be accurately tessellated into 3D volume. The diamond and the fluorite lattices do have nodes in the interior of the tessellation volume and represent a significant spread in compliance (Supplementary Figure 6). The requirement to ensure nodes are not on the tessellation boundaries can however be overcome by shifting the tessellation volume to move nodes into its interior and redefining the unit cell. Another alternative is to hybridize[32] a unit cell such as the FCC, which does have nodes on the tessellation surface, with a latticelike the BCC, which does not. This hybrid lattice thus confines the FCC cell within BCC cells and periodicity is obtained with the unit cell now becoming a hybrid collection of FCC and BCC cells (Supplementary Figure 7). The prior experiment with BCC lattices was repeated with these three additional lattice structures, and similar observations made as with the BCC (Fig. 4a, b): a clear increase in effective compliance was observed, along with a smoothening of the plateau region (Supplementary Movies 2–4).

The experimentally obtained normalized effective modulus (E^*/E_s), which is the inverse measure of compliance, of each of the four traditional lattices and their interwoven counterparts is plotted in Fig. 4c as a function of their relative densities (ρ^*/ρ_s), where E^* and ρ^* represent Young's modulus and relative density of the lattice respectively, and E_s and ρ_s represent the corresponding properties of the base material. For all four lattice shapes, between a 4- and 21-fold increase in compliance is observed, depending on cell type (Supplementary Figure 8). This is particularly remarkable given that the traditional BCC, diamond, and fluorite topologies are among the most compliant unit cell structures available in the library of commonly used lattice shapes (Supplementary Figure 6).

The normalized effective modulus is related to relative density via a power-law relationship as:[3]

$$\frac{E^*}{E_s} = C\left(\frac{\rho^*}{\rho_s}\right)^m \qquad (1)$$
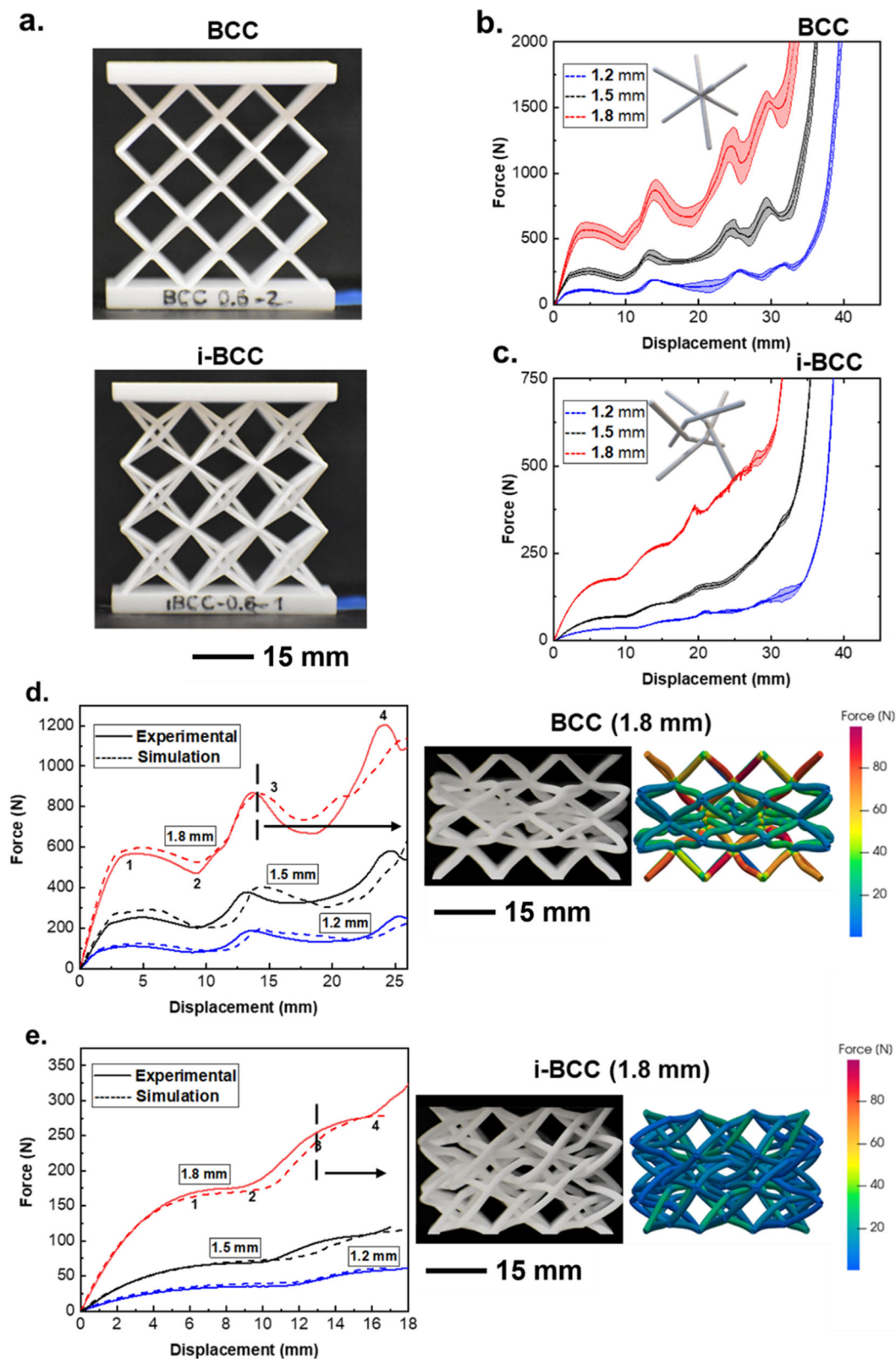
Fig. 3 Comparison of mechanical behavior of traditional and interwoven BCC lattices under compression. a Undeformed BCC and i-BCC lattices made of Nylon-12 using selective laser sintering; **b** force-displacement response under compression for a traditional BCC structure with three different strut thicknesses; **c** and for an i-BCC, showing a far more compliant response with fewer undulations; comparisons to simulation for **d** traditional BCC and **e** i-BCC, showing good agreement and demonstrating differences in homogeneity of internal force distribution within the struts at 30% global effective strain (corresponding to a 13 mm displacement).
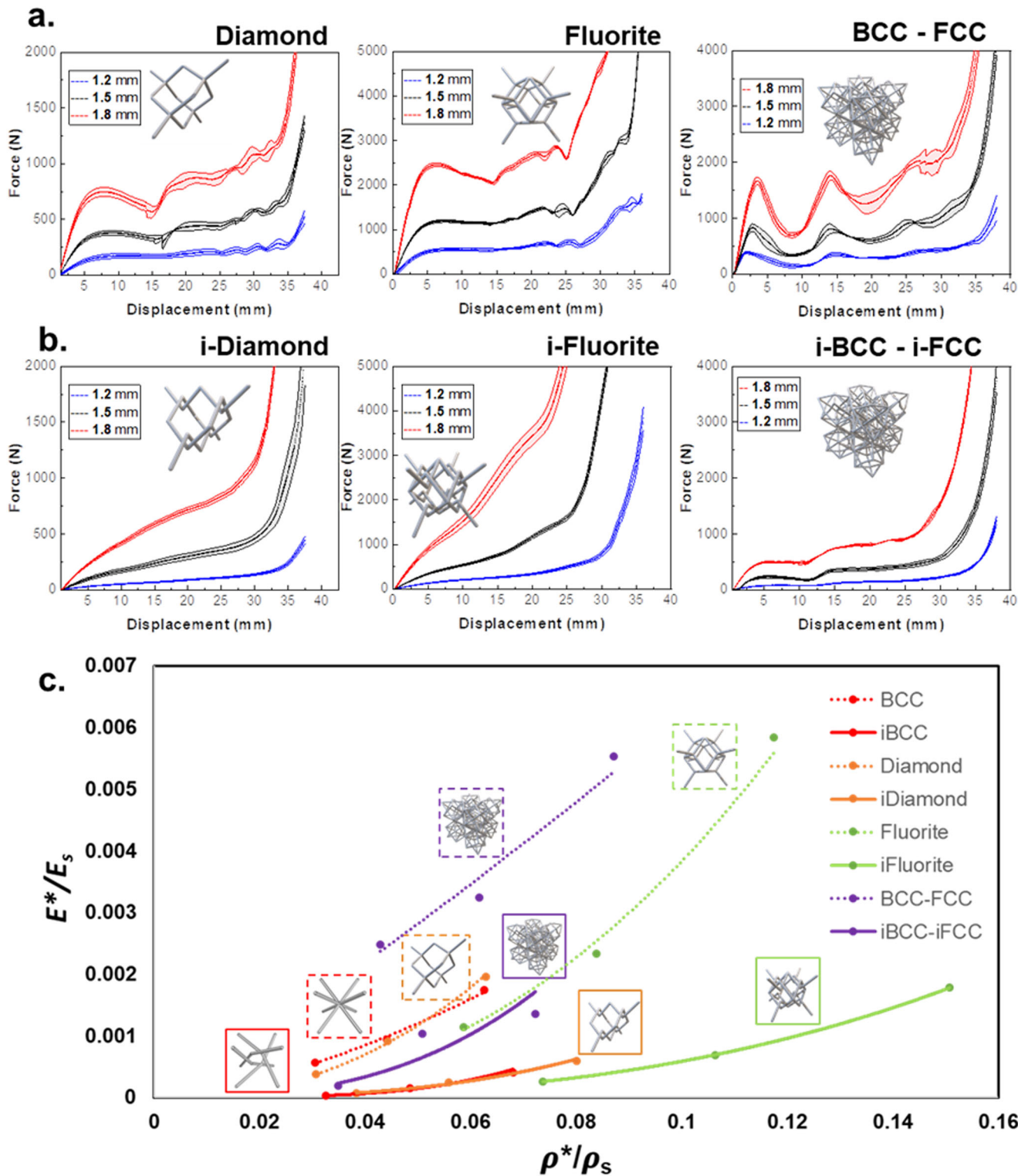
Fig. 4 Comparison of the mechanical response and effective modulus between traditional and interwoven lattices under compression. Compression force-displacement responses for **a** traditional; and **b** interwoven diamond, fluorite, and a hybrid BCC-FCC structure with three replicates for each design; **c** normalized effective modulus against relative density for all four lattice shapes studied demonstrates the generality of the observation of increased compliance.

where C and m are unit cell topology-specific parameters. Stretch-dominated lattices have an exponent m value that is approximately 1, with bending-dominated lattices and open cell foams having an exponent value close to 2, though in reality these are typically established experimentally and show some variation

depending on unit cell shape[3]. A higher exponent value indicates higher compliance for a given relative density (this is due to the fact that relative density of a cellular material is always <1). The C and m parameters derived for the four lattice types in this work for both traditional and interweaving designs are listed in Table 1.

Decoupling nodes to create an interweaving lattice thus clearly has the effect of significantly increasing the value of the exponent, as much as doubling it for the BCC and BCC-FCC hybrid structures.

Another method of explaining the behavior of interwoven lattices relative to their traditional counterparts is to interpret them in the context of Maxwell's criterion[33], as generalized by Calladine for three-dimensional structures[34], as:

$$b - 3j + 6 = s - m \qquad (2)$$

Here, b and j represent the number of struts and frictionless joints in an assumed pin-jointed frame, and s and m are counts of the states of self-stress and mechanisms, respectively. A just-rigid framework has $s = m = 0$[28], but for bending-dominated structures, $s-m$ is a negative number. Interweaving a lattice has the effect of creating additional joints where the struts kink, while keeping the number of struts the same, thus making $s-m$ an even smaller number, indicating an increase in the number of available mechanisms for deformation (Supplementary Figure 10). This effectively indicates that interweaving a lattice has the effect of making it more bending-dominated and could thus be used to enhance deformability of even stiff, stretch-dominated lattices. While the material used for this study (Polyamide-12) has very different properties compared to the silica that comprises the Venus flower basket, the underlying principle that enables higher compliance is expected to be widely applicable across a range of material compositions.

Table 1 Comparison of power-law parameters for traditional and interweaving lattices studied.

	Traditional			Interweaving		
	C	m	R²	C	m	R²
BCC	0.13	1.56	0.99	10.06	3.72	0.98
Diamond	1.26	2.33	0.99	0.96	2.91	0.99
Fluorite	0.84	2.34	0.99	0.30	2.71	0.99
BCC-FCC	0.08	1.12	0.96	2.49	2.77	0.77

C and m are unit cell topology-specific parameters and the R^2 value is a measure of the quality of the power-law fit.

Discussion

To examine interwoven lattices beyond the context of this study, and compare their stiffness responses to other cellular materials, an Ashby plot for normalized effective modulus was developed and is shown in Fig. 5. To meaningfully compare moduli with data from the literature, it is essential to minimize edge-effects which can accompany structures with only a few cells in them. Thus, following ISO 13314[35], additional BCC and i-BCC lattice structures with 10 cells in each direction were designed, fabricated, and tested (Supplementary Figs. 11–13).

Figure 5 shows key categories of cellular materials grouped, with special emphasis on different design approaches to 3D woven cellular materials in the literature. With the exception of the braided strut lattices[27], the interwoven lattices from this work are the most compliant structures at a given relative density. Unlike the very high-resolution additive manufacturing process necessary to generate braided struts, selective nodal decoupling does not impose significantly more stringent manufacturing requirements than the traditional counterparts from which they are derived, though they may drive the need for support structures with some processes such as Fused Deposition Modeling and Stereolithography.

Conclusions

This work has, inspired by a design principle observed in the Venus flower basket, introduced a class of lattice materials designed by selectively decoupling nodes within the lattice unit cell tessellation volume. This work has also shown how this decoupling leads to significant increases in compliance under compression, even for already compliant bending-dominated lattices. It has implications for the design of compliant architected cellular materials with applications in piezoelectric sensing for wearables and biomedical devices[36,37], energy absorbers[38], vibration damping[24], and other applications where high compliance is sought at large relative densities. It also suggests further exploration of interwoven designs for surface-based structures like those derived from Triply Periodic Minimal Surface geometries[39,40]. This work also suggests two levels of further optimizing the lattice design for compliance—at a local level, this can be done by the modulation of the interweaving distance, at a global level, nodes can be decoupled only in certain locations where increases in compliance are sought. Finally, while this work has not explicitly modeled the cylindrical structure of the Venus
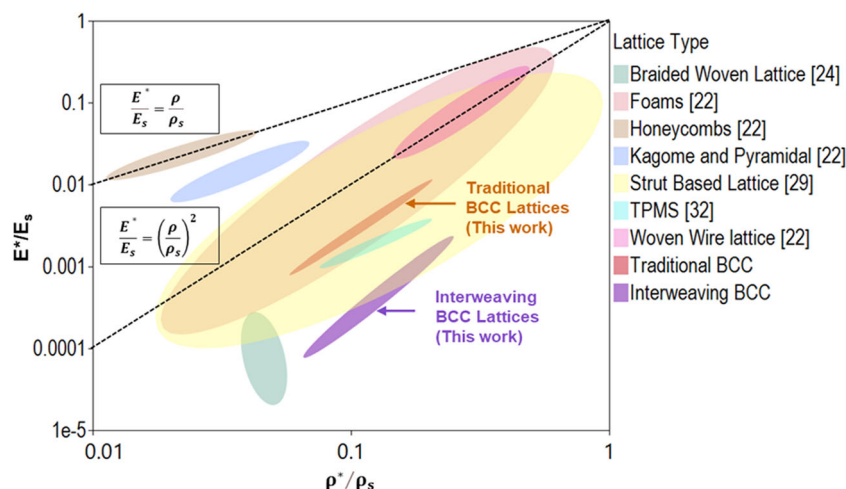
Fig. 5 Ashby chart showing normalized effective modulus for several cellular solids from the literature[41-43]. This includes the woven configurations[27,42]. Results from the traditional and interwoven 10 × 10 × 10 lattices developed in this work are shown aggregated within the indicated bubble.

flower basket, it may be speculated that the reduction in internal forces and increase in structural compliance that is associated with nodal decoupling may contribute to the organism's resilience in its early stages of growth before the strengthening mechanisms of diagonal weaves, helical ridges and nodal fusion have fully developed[12], though more work is needed to establish the validity of this claim.

Methods

X-ray tomography of venus flower basket. Venus flower basket specimen was obtained online from Etsy.com and is widely available on this, and similar sites. The multiscale structure of the Venus flower basket was investigated using a commercial x-ray microscope (Zeiss Xradia Versa 620, Thornwood, NY). Multiple scans with pixel size ranging from 23.5 µm to 8.4 µm were performed to probe the structure varying length scales. Post scanning, all the 3D datasets have been processed in a commercial image analysis software (Avizo 9.0, Bethesda, MD) for visualization and further analysis. Further details on tomography setup and findings can be found in Morankar et al.[11].

Design. All designs in this study were created using the Rhino 7 software (Robert McNeel & Associates) with a Grasshopper plugin. Supplementary Figures 14-17 show the grasshopper code which converts traditional lattice into interwoven lattice, with code available on an online repository[29]. The inputs are, unit cell size (15 mm), interweaving distance (3 mm) and number of cells (3 in each direction) were kept constant across all three designs. Three variations of the strut diameter are considered for each design, i.e., 1.2 mm, 1.5 mm, and 1.8 mm. A 3x2x3 DoE plan was generated and three instances for each design type were printed for repeatability.

Four steps were used to obtain an interwoven lattice design from a traditional one:

1. Identify and separate the two planes which contain struts with intersecting nodes. blue (ABGH) and red (CDEF)
2. Taking one plane at a time (ABGH), draw a line starting at the intersection (Red Dot) with distance d and -d (Interweaving Distance) in perpendicular direction to the respective plane forming i1 and i2 points. This are the interweaving or decoupled points.
3. Join Bi1H and Ai2G to form an interwoven node.
4. Repeat the same procedure for red plane (CDEF) and then combine the two results together to form an interwoven BCC unit cell (i-BCC).

The process for interweaving Fluorite and Diamond is more complex than BCC as they contain a greater number of intersecting nodes, but the general process of identifying the intersecting strut's plane and using its perpendicular direction to form an interweaving node is same for all the structures. Certain rules are to be considered while interweaving any given structure:

- Only lattices with nodes in interior of the unit cell can be interweaved by the above-described method, as the surficial nodes will hinder the other nodes of the unit cell when stacked in a grid system.
- All the nodes within the original unit cell should remain in the unit cell volume after decoupling.
- The max interweaving distance is defined by:
  - Whether the decoupled node hinders with any other node
  - Whether the decoupled node stays within the original unit cell volume

- The interweaving distance should be greater than then minimum resolution of the 3D printer to avoid the merging of struts when printed.

Manufacturing. (Supplementary Figure 2) shows all the printed lattices. The specimens were additively manufactured using Selective Laser Sintering on a EOS FORMIGA P 110 3D printer with PA12 (Nylon-12) as the material. Printed specimens were measured using a vernier caliper to verify strut diameters. The measurements had an average error of 5.25%, which is not that significant and hence was ignored in modeling and simulations.

Testing. All the specimens were tested in compression on a Instron 5985 testing machine with a 250 kN load cell. The compression displacement rate was set to be 1 mm per second (effective strain rate of 0.02 per sec) and the compression was done till densification. (Supplementary Figure 9) of the supplementary material shows the deformation of all the specimens at different strain values. The main goal here was to extract load displacement data for each specimen and compute their compliance. A Digital SLR camera was used to capture video recordings during compression, which were used to extract the still images. Time synchronization was used to establish the strain. The compliance was computed by using the inverse of the stiffness taken from the linear elastic regime of the load displacement curves.

Simulation. The simulation results reported in Fig. 2d, e, as well as Supplementary Figs. 4 and 5, were obtained using a nonlinear (geometrically exact), shear-deformable 3D beam model with linear elastic-viscoplastic material behavior[31]. First, the material behavior of the 3D printed PA12 was characterized by uniaxial tension tests at various strain rates. Subsequently, a simple linear elasto-visco-plastic material model analogous to a rheological 1-D generalized Maxwell model with an elasto-plastic branch and a visco-elastic branch in parallel was fitted to the experimental curves, obtaining a satisfactory agreement (Supplementary Figure 3). This material model was then used in a B-Spline based isogeometric collocation method for the numerical discretization of the 3D beam structures, which were carried out in a C++ code[31]. For this purpose, the geometric descriptions of the i-BCC designs were directly imported from Rhino/Grasshopper into this code. To ensure convergence in the presence of instabilities, small randomized geometric perturbations were applied to the strut geometries. The nonlinear simulations of the compression tests were then executed by constraining the bottom nodes of the structures and incrementally applying uniform displacements to all top nodes at the experimental rate of 1 mm per second. In this processes, beam-to-beam contacts were also considered using a penalty method.

Data availability

Supplementary material includes additional figures and a table referenced in this work. Experimental and simulation data is available from the corresponding author upon request.

Code availability

Grasshopper scripts developed in Rhinoceros 7 for all four designs in this work have also been made available at an open repository and can be accessed here: https://doi.org/10.5281/zenodo.7863359. Supplementary Figs. 14–17 provide additional background on these files. Additional information regarding these scripts is available from the corresponding author upon reasonable request.

References

1. Yu, X., Zhou, J., Liang, H., Jiang, Z. & Wu, L. Mechanical metamaterials associated with stiffness, rigidity and compressibility: a brief review. *Prog. Mater. Sci.* **94**, 114–173 (2018).
2. Berger, J. B., Wadley, H. N. G. & McMeeking, R. M. Mechanical metamaterials at the theoretical limit of isotropic elastic stiffness. *Nature* **543**, 533–537 (2017).
3. Gibson, L. & Ashby, M. Cellular Solids: Structure and Properties. (1999).
4. Bhate, D. et al. Classification and selection of cellular materials in mechanical design: engineering and biomimetic approaches. *Designs* **3**, 19 (2019).
5. Penick, C. A. et al. The comparative approach to bio-inspired design: integrating biodiversity and biologists into the design process. *Integr. Comp. Biol.* (2022) https://doi.org/10.1093/icb/icac097.
6. Goss, D. et al. Bio-inspired honeycomb core design: an experimental study of the role of corner radius, coping and interface. *Biomimetics* **5**, 59 (2020).
7. Rajeev, A. et al. Parametric optimization of corner radius in hexagonal honeycombs under in-plane compression. *J. Manuf. Process.* **79**, 35–46 (2022).
8. du Plessis, A. et al. Properties and applications of additively manufactured metallic cellular materials: a review. *Prog. Mater. Sci.* **125**, 100918 (2021).
9. Bhate, D. Four questions in cellular material design. *Materials* **12**, 1060 (2019).
10. Plocher, J. & Panesar, A. Review on design and structural optimisation in additive manufacturing: towards next-generation lightweight structures. *Mater. Des.* **183**, 108164 (2019).
11. Morankar, S. et al. Tensile and Fracture behavior of Silica Fibers from the Venus Flower Basket (Euplectella aspergillum). *Int. J. Solids Struct.* **253**, 111622 (2022).
12. Weaver, J. C. et al. Hierarchical assembly of the siliceous skeletal lattice of the hexactinellid sponge Euplectella aspergillum. *J. Struct. Biol.* **158**, 93–106 (2007).
13. Tavangarian, F., Sadeghzade, S. & Davami, K. A novel biomimetic design inspired by nested cylindrical structures of spicules. *J. Alloys Compd.* **864**, 158197 (2021).
14. Fernandes, M. C., Aizenberg, J., Weaver, J. C. & Bertoldi, K. Mechanically robust lattices inspired by deep-sea glass sponges. *Nat. Mater.* **20**, 237–241 (2021).
15. Fernandes, M. C. et al. Mechanical and hydrodynamic analyses of helical strake-like ridges in a glass sponge. *J. R. Soc. Interface* **18**, 20210559 (2021).

16. He, M. et al. Compressive performance and fracture mechanism of bio-inspired heterogeneous glass sponge lattice structures manufactured by selective laser melting. *Mater. Des.* **214**, 110396 (2022).

17. Li, Q. & Sun, B. How to surpass the deep-sea glass sponges mechanically. 1–11 (2021) https://doi.org/10.20944/preprints202112.0042.v1.

18. Sharma, D. & Hiremath, S. S. Bio-inspired repeatable lattice structures for energy absorption: Experimental and finite element study. *Compos. Struct.* **283**, 115102 (2022).

19. Baumeister, D. & Smith, J. Biomimicry Resource Handbook: A Seed Bank of Best Practices. (CreateSpace Independent Publishing Platform), (2014).

20. Sadeghzade, S., Emadi, R., Salehi, M., Tavangarian, F. & Ramini, A. Crack propagation and toughening mechanisms of bio-inspired artificial spicules fabricated by additive manufacturing technique. *Theor. Appl. Fract. Mech.* **110**, 102797 (2020).

21. Bilisik, K., Karaduman, N. S., Bilisik, N. E. & Bilisik, H. E. Three-dimensional fully interlaced woven preforms for composites. *Text. Res. J.* **83**, 2060–2084 (2013).

22. Keefe, E. M., Thomas, J. A., Buller, G. A. & Banks, C. E. Textile additive manufacturing: An overview. *Cogent. Eng.* **9**, 2048439 (2022).

23. Ha, S. H., Lee, H. Y., Hemker, K. J. & Guest, J. K. Topology optimization of three-dimensional woven materials using a ground structure design variable representation. *J. Mech. Des. Trans. ASME* **141**, 061403 (2019).

24. Salari-Sharif, L. et al. Damping of selectively bonded 3D woven lattice materials. *Sci. Rep.* **8**, 6–11 (2018).

25. Zhang, Y. et al. Fabrication and mechanical characterization of 3D woven Cu lattice materials. *Mater. Des.* **85**, 743–751 (2015).

26. White, B. C., Garland, A., Alberdi, R. & Boyce, B. L. Interpenetrating lattices with enhanced mechanical functionality. *Addit. Manuf.* **38**, 101741 (2021).

27. Moestopo, W. P., Mateos, A. J., Fuller, R. M., Greer, J. R. & Portela, C. M. Pushing and pulling on ropes: hierarchical woven materials. *Adv. Sci.* **7**, 1–8 (2020).

28. Deshpande, V. S., Ashby, M. F. & Fleck, N. A. Foam topology: Bending versus stretching dominated architectures. *Acta Mater* **49**, 1035–1040 (2001).

29. Bhate, D. & Mistry, Y. Grasshopper Scripts for Bio-Inspired Selective Nodal Decoupling for Ultra-Compliant Interwoven Lattices. (2023) https://doi.org/10.5281/zenodo.7863359.

30. Gibson, I., Rosen, D. & Stucker, B. *Additive Manufacturing Technologies*. (Springer), (2015).

31. Weeger, O., Schillinger, D. & Müller, R. Mixed isogeometric collocation for geometrically exact 3D beams with elasto-visco-plastic material behavior and softening effects. *Comput. Methods Appl. Mech. Eng.* **399**, 115456 (2022).

32. Ramirez-chavez, I. E., Anderson, D., Sharma, R., Lee, C. & Bhate, D. A classification of aperiodic architected cellular materials. *Designs* **6**, 63 (2022).

33. Maxwell, J. C. On reciprocal figures and diagrams of forces. *Philos. Mag.* **4**, 250–261 (1864).

34. Calladine, C. R. Buckminster Fuller's 'Tensegrity' structures and Clerk Maxwell's rules for the construction of stiff frames. *Int. J. Solids Struct.* **14**, 161–172 (1978).

35. ISO. ISO 13314: Mechanical testing of metals, ductility testing, compression test for porous and cellular metals. 13314 (2011).

36. Cui, H. et al. materials with designed anisotropy and directional response. *Nat. Mater.* **18**, 234–241 (2019).

37. Liu, S. et al. Continuous three-dimensional printing of architected piezoelectric sensors in minutes. *Research* **2022**, 9790307 (2022).

38. Shinde, M. et al. Towards an ideal energy absorber: relating failure mechanisms and energy absorption metrics in additively manufactured AlSi10Mg cellular structures under quasistatic compression. *J. Manuf. Mater. Process.* **6**, 140 (2022).

39. Zhang, C. et al. Mechanical responses of sheet-based gyroid-type triply periodic minimal surface lattice structures fabricated using selective laser melting. *Mater. Des.* **214**, 110407 (2022).

40. Yang, L. et al. Tailorable and predictable mechanical responses of additive manufactured TPMS lattices with graded structures. *Mater. Sci. Eng. A* **843**, 143109 (2022).

41. Chen, S. et al. A novel composite negative stiffness structure for recoverable trapping energy. *Compos. Part A Appl. Sci. Manuf.* **129**, 105697 (2020).

42. Ashby, M. The properties of foams and lattices. *Philos. Trans. R. Soc. A Math. Phys. Eng. Sci.* **364**, 15–30 (2006).

43. Ashby, M. F. et al. *Metal Foams: A Design Guide*. (Butterworth Heinemann), (2010).

Author contributions

Y.M. developed the design methods in this work and conducted all experimental testing in this work. D.B. supervised Y.M. S.M. performed X-ray micro tomography on the Venus Flower Basket. N.C. supervised S.M. O.W. conducted simulation of the BCC and i-BCC structures. M.S. performed compression tests and performed simulation analyses on different cell topologies to identify best candidates for study in this work. C.P. provided biological information on the Venus Flower Basket and sourced a specimen for X-ray microtomography scan. D.B., N.C., and C.P. secured funding to support this work. X.C. and S.L. developed the notion of ultra-compliance as the key output of this study through their evaluation of this structure in the context of a specific application currently under study. Y.M. and D.B. co-wrote the first draft of this paper, all authors provided revisions. Revisions and editorial changes were made by Y.M. and D.B.

Competing interests

Portions of this work have formed the basis for a provisional US patent application titled "Method for Designing Ultra-Compliant Interwoven Meta-Materials," # 63/375,808, filed on 09/15/2022, with authors Y.M., S.L., M.S., X.C., D.B., S.M., N.C., and C.P. All other authors declare no competing interests.

Additional information

Supplementary information The online version contains supplementary material available at https://doi.org/10.1038/s43246-023-00363-6.

Correspondence and requests for materials should be addressed to Dhruv Bhate.

Peer review information *Communications Materials* thanks the anonymous reviewers for their contribution to the peer review of this work. Primary Handling Editors: Jet-Sing Lee and John Plummer. A peer review file is available

Reprints and permission information is available at http://www.nature.com/reprints

Publisher's note Springer Nature remains neutral with regard to jurisdictional claims in published maps and institutional affiliations.